Role of incomplete fusion of the projectile in the $^{16}O + ^{115}In$ interaction at low energies

Kamal Kumar,[1,*] Tauseef Ahmad,[1] Sabir Ali,[1] I. A. Rizvi,[1,†] Avinash Agarwal,[2] R. Kumar,[3] and A. K. Chaubey[4]

[1]*Department of Physics, Aligarh Muslim University, Aligarh, Uttar Pradesh 202 002, India*

[2]*Department of Physics, Bareilly College, Bareilly, Uttar Pradesh 243 005, India*

[3]*NP-Group, Inter University Accelerator Centre, New Delhi 110 067, India*

[4]*Department of Physics, Addis Ababa University, P.O. Box 1176, Addis Ababa, Ethiopia*

(Received 13 February 2014; revised manuscript received 30 March 2014; published 21 May 2014)

Complete and incomplete fusion of an ^{16}O projectile with an ^{115}In target is studied. Forward recoil range distributions of several evaporation residues were measured at 105 MeV beam energy. The recoil catcher activation technique followed by offline gamma ray spectroscopy was used. The disentanglement of the complete and incomplete fusion processes was done in terms of full and partial linear momentum transfer from the projectile to the target nucleus. Results indicate the occurrence of incomplete fusion involving the breakup of ^{16}O into $^{4}He + ^{12}C$ and/or $^{8}Be + ^{8}Be$ followed by fusion of one of the fragments with the target nucleus ^{115}In. The complete fusion contributions deduced from the recoil range distribution data were found to be consistent with the predictions of the theoretical model code PACE4. An attempt was also made to separate out the relative contributions of complete and incomplete fusion components from the analysis of the measured recoil range distribution data. The study indicates that the incomplete fusion contribution increases with the projectile energy and the mass asymmetry of the interacting partners. The projectile structure effect also plays an important role in the underlying reaction dynamics.

DOI: 10.1103/PhysRevC.89.054614 PACS number(s): 25.70.Jj, 25.70.Gh, 25.70.Mn

I. INTRODUCTION

The understanding of low-energy incomplete fusion (ICF) is a topic of current interest due to the lack of proper theoretical aspects [1–6]. These studies have benefitted from the availability of radioactive ion beams, which are very significant for understanding reactions of astrophysical interest and for the production and study of new isotopes of existing nuclei [7–13]. Moreover, ICF has also been observed near the Coulomb barrier (CB) where complete fusion (CF) is expected to be the sole contributor to the total reaction cross section [14–17].

It is now a widely accepted fact that at energies near and/or beyond the Coulomb barrier, the unambiguous reaction processes are the formation and decay of an equilibrated compound nucleus (CN) followed by the entire projectile's fusion with the target nucleus [3–5], leading to the amalgamation of all nucleonic degrees of freedom of these interacting partners. However, ICF has been found to be competing fusion-like process at energies even a little above the Coulomb barrier [18–20], forming a reduced excited composite system with relatively lower mass, charge, and excitation energy compared to the completely fused composite system, due to the prompt emission of forward-peaked projectile-like fragments (PLFs) at the initial stage of interaction. These reactions were first observed by Britt and Quinton [21] and Galin *et al.*, [22]. The study of ICF by particle-gamma coincidence measurements [23] has also contributed significantly to the understanding of the mechanism of these reactions.

Several models have been proposed to explain the ICF reaction dynamics, such as hot spot model [24], sum rule model [25], breakup fusion model [26], exciton model [27], and promptly emitted particles model [28]. All these models have been used to fit the experimental data obtained using projectile energies above 10 MeV/nucleon. However, Parker *et al.* [29] observed forward-peaked α particles in low-Z heavy-ion interactions on a ^{51}V target at energies 6 MeV/nucleon. Moreover, the existence of ICF at low incident energies and/or below the values of ℓ_{crit} (for CF) has been claimed in recent studies [30–32], contrary to the hypothesis of an angular momentum window in the sum rule model of Wilczynski *et al.* [25]. As the projectiles ^{12}C, ^{16}O, and ^{20}Ne are clusters of α particles, it could be assumed that it is easy to transfer an α particle from these projectiles to the target. In such reactions the mass flow is always from projectile to target. Further, Ahmad *et al.* [33] and Agarwal *et al.* [12], by their excitation function and recoil range distribution studies, have clearly shown the significant contribution of ICF in the production of α emission channels. In Ref. [34], the incomplete fusion probability is predicted to be almost proportional to the target charge Z_T. Moreover, the projectile structure and the α-Q value of the projectile were also found to be responsible for the ICF contribution [30,35,36]. Hence, the observation of ICF reaction dynamics at low energies, especially its dependence on different entrance channel parameters, makes the study more important. Therefore, the study of degree of fusion incompleteness, i.e., the degree of linear momentum transfer (LMT) associated with CF and ICF was carried out, and the relative contributions of CF and ICF were extracted. In the present work, in order to facilitate the experimental disentanglement of these competing processes (CF and ICF), the forward recoil range distributions (FRRDs) of the reaction residues populated in the $^{16}O + ^{115}In$ interaction at beam

*kamalkumar1908@gmail.com

†isarrizvi@hotmail.com

energy 105 MeV were measured. The target ^{115}In was chosen because many of the possible evaporation residues produced in this interaction have half-lives and decay properties suitable for offline measurement. Moreover, an attempt was also made to obtain quantitative information on ICF reactions. The present work is in continuation of our recent investigation of the same system, ^{16}O + ^{115}In [30], where the measurement and analysis of excitation functions was done to investigate the role of breakup processes in ICF reaction dynamics.

II. EXPERIMENTAL PROCEDURE

The experiment was carried out at the Inter University Accelerator Centre (IUAC), New Delhi, India. A stack consisting of targets ^{115}In (abundance = 95.7%) and ^{113}In (abundance = 4.3%) followed by a series of fifteen thin Al-catcher foils, to trap the recoiling residues, was irradiated separately by an ^{16}O beam of 105 MeV energy. The irradiation time of around 12 h with a beam current ≈3 p nA was selected according to the half-lives of the radioisotopes produced. The irradiation was done in the general purpose scattering chamber (GPSC) using the in-vacuum transfer facility (ITF). A Faraday cup was placed behind the target-catcher assembly to collect the total charge. The target ^{115}In was mounted in such a way that the Al backing first faced the beam so that the recoiling nuclei, if any, of very short range did not stop in the target thickness itself. Hence, an energy loss of 3.7 MeV takes place in the target backing, and the incident energy on the target is estimated to be 101.3 MeV. The contribution due to the low-abundant ^{113}In in the target was rejected, as it is considerable only at low energies. The thicknesses of each target and catcher foil were separately measured through weighing and by an α-transmission method, respectively. The thickness of the target was ≈199 μg/cm^2; however, the thicknesses of Al catchers were ≈65–90 μg/cm^2. A typical experimental arrangement is shown in Fig. 1.

The activities produced in each Al-catcher foil of the stack were counted separately using a high-purity germanium (HPGe) detector of 100 cm^3 active volume coupled with the computer-automated measurement and control (CAMAC) based CANDLE [37] software. The detector was precalibrated both for energy and efficiency using a standard γ source, ^{152}Eu.

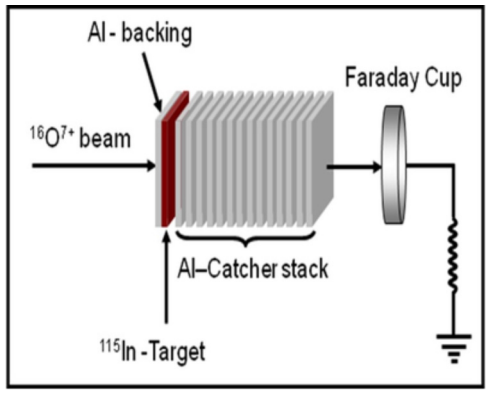

FIG. 1. (Color online) A typical stack arrangement used for the measurement of forward recoil ranges of reaction products.

TABLE I. List of reactions with their residues and spectroscopic properties.

Residue	$T_{1/2}$	J^π	E_γ (keV)	I^γ
^{127}Ba($p3n$)	12.7 min	$1/2^+$	180.8	12.0
			114.8	9.3
^{126}Ba($p4n$)	100.0 min	0^+	233.6	19.6
^{127}Cs(α)	6.25 h	$1/2^+$	411.8	63.0
^{125}Cs($\alpha 2n$)	45.0 min	$1/2^+$	526.0	24.0
			111.8	9.0
^{125}Xe(αpn)	16.9 h	$1/2^+$	188.4	54.0
^{123}Xe($\alpha p3n$)	2.08 h	$1/2^+$	148.9	49.0
			178.1	14.9
^{122}Xe($\alpha p4n$)	20.1 h	0^+	350.0	7.8
^{121}I($2\alpha 2n$)	2.12 h	$5/2^+$	212.2	84.0
^{120}I^g($2\alpha 3n$)	81.0 min	2^-	560.4	73.0
			601.1	5.8
^{120}I^m($2\alpha 3n$)	53.0 min	4 to 8	560.4	100.0[a]
			601.1	87.0[a]
^{119}I($2\alpha 4n$)	19.1 min	$5/2^+$	257.5	87.0[a]
^{118}Sb^m($3\alpha n$)	5.00 h	8^-	1050.0	97.0[a]
			1229.0	100.0[a]
^{117}Sb($3\alpha 2n$)	2.80 h	$5/2^+$	158.5	86.0[a]
^{116}Sb^m($3\alpha 3n$)	60.3 min	8^-	1293.5	100.0[a]
			972.6	74.2[a]

[a]These intensities are relative.

The resolution of the HPGe detector was found to be 2 keV for 1408 keV γ ray of the ^{152}Eu source, during the counting of the samples. The γ-ray spectra of each foil were recorded at increasing times so that the decay-curve analysis could be done to verify the half-lives and identification of the residues. The measured half-lives of the residues were found to be in good agreement with the literature values [38]. A list of identified reaction residues populated in the ^{16}O + ^{115}In interaction are tabulated in Table I, along with their spectroscopic properties [38].

III. ESTIMATION AND ANALYSIS OF FRRDS

To measure the relative contributions of CF and ICF reaction processes, in the interaction of ^{16}O with ^{115}In, FRRDs of several evaporation residues were obtained. The measurement of the projected ranges of the reaction products depends on the degree of linear momentum transfer (ρ_{LMT}) from the projectile to the target nucleus, and thus on the mass of projectile fused with the target. This is a well established method to distinguish CF and/or ICF reactions. The velocity distribution of the evaporated residues is symmetric about their most probable velocity v_o. The standard deviation of the velocity distribution depends on the particles evaporated from the equilibrated CN. The mean velocity v_o may be given as

$$v_o = v_{CN} = \frac{\sqrt{2M_P E}}{M_{P+T}}, \quad (1)$$

where M_P is the projectile mass, M_{P+T} is the total mass of the composite system (projectile+target), and E is the projectile energy. Moreover, the degree of linear momentum transfer

may be given as

$$\rho_{LMT} = \frac{P_{\text{frac}}}{P_{\text{proj}}}, \tag{2}$$

where P_{frac} is the linear momentum due to the fused fraction of the projectile, and P_{proj} is the total linear momentum of the projectile. As linear momentum is proportional to the fused mass of the projectile, hence the longest projected range can be assigned to the entire fusion of the projectile to the target. Since, in CF process, the target gets the maximum linear momentum from the projectile, therefore, for a given interaction the CN has predetermined mass, energy, and momentum. However, in the case of ICF, due to availability of different degrees of linear momentum transfer, the mass, energy, and momentum of the composite system may not have unique values. This may result from the fluctuations in the fused mass from the projectile to the target nucleus. Therefore, the experimentally measured forward recoil ranges of the final reaction products in the stopping medium give information about the ρ_{LMT} involved.

The trapped recoiling reaction products in the catcher foils were identified by their characteristic γ radiation on the basis of their half-lives. The production cross sections σ_R(E) for the identified reaction products were computed using the standard formulation given in Ref. [14]. The normalized yield is obtained by dividing the cross section of the reaction products in each catcher foil by its thickness. The resulting normalized yields were plotted against cumulative catcher foil thicknesses to obtain the recoil range distributions for the identified residues, viz., ^{127}Ba($p3n$), ^{126}Ba($p4n$), ^{127}Cs(α), ^{125}Cs($\alpha 2n$), ^{125}Xe(αpn), ^{123}Xe($\alpha p3n$), ^{122}Xe($\alpha p4n$), ^{121}I($2\alpha 2n$), ^{120}I^{g}($2\alpha 3n$), ^{120}I^{m}($2\alpha 3n$), ^{119}I($2\alpha 4n$), ^{118}Sb^{m}($3\alpha n$), ^{117}Sb($3\alpha 2n$), and ^{116}Sb^{m}($3\alpha 3n$). Figures 2(a) and 2(b) show the recoil range distributions of residues ^{127}Ba and ^{126}Ba at beam energy 105 MeV. The accuracy of these distributions was limited by the uncertainity in determining the catcher thickness, generally about 5%. The size of the circles in all recoil range distributions includes the uncertainty in the yield values. In Fig. 2(a), for the $p3n$ channel, the measured RRD shows only one peak at a depth 1003 μg/cm^2, indicating only a single linear momentum transfer component, which is a characteristic of the CF process involved in the production of ^{127}Ba. Further, the width of the peak reflects the perturbing effects of the evaporation of nucleons on the recoil velocity of the product, combined with the effects of straggling. The identified reaction products and their experimentally measured most probable ranges R_P^{expt} in the stopping medium, for both the CF residues, along with their theoretically estimated (using the code SRIM [39]) mean ranges R_P^{theor} in the stopping medium, are given in Table II. The most probable recoil ranges (R_P^{theor}) were calculated assuming that, in the case of CF, the entire nucleonic degrees of freedom of projectile and target amalgamate, and hence the projectile transfers its total linear momentum to the target, which recoils to conserve the linear momentum. An attempt was also made to observe the pertubing effects of the evaporation nucleons in the full widths at half maximum (FWHM) of the

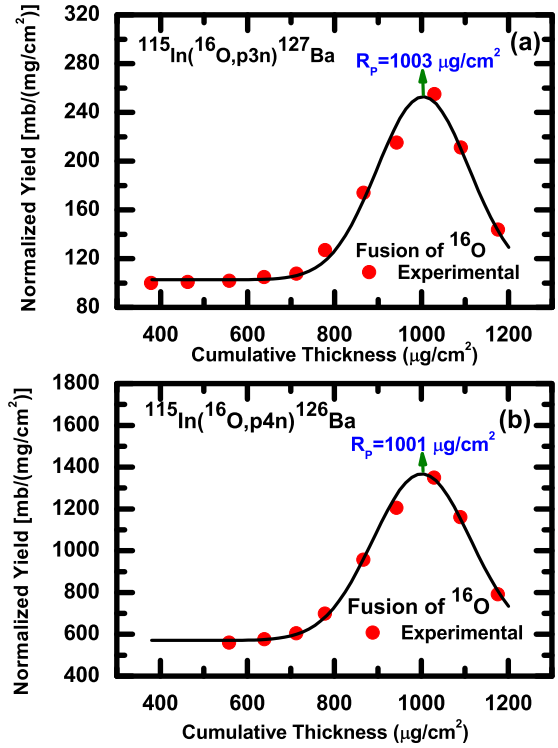

FIG. 2. (Color online) The experimentally measured recoil range distributions of (a) ^{127}Ba ($p3n$) and (b) ^{126}Ba ($p4n$) produced in the ^{16}O + ^{115}In system at 105 MeV energy.

observed FRRDs. The normalized FWHM (FWHM/R_P^{expt}) were deduced for the observed distributions, and are tabulated in Table III. The normalized FWHM are consistent for the CF and ICF residues individually. As a representative case, for the ^{119}I($2\alpha 4n$) residue, the peak resolution for CF is 0.06, while for ICF-α and ICF-2α the peak resolution increases to 0.18 and 0.44, respectively, as expected. It is clear from the above that the population of reaction product ^{127}Ba produced via the $p3n$ channel is associated with the entire linear momentum transfer from the projectile to the target nucleus, and may be represented as

$$^{16}O + {}^{115}\text{In} \Rightarrow {}^{131}\text{La}^{*} \Rightarrow {}^{127}\text{Ba} + p3n,$$

In a similar way, the FRRD for the residue ^{126}Ba($p4n$) was found to have a single peak showing complete linear momentum transfer from the projectile to the target, indicating the production of this residue via CF process only. The experimentally measured mean range for this residue is listed in Table II. Further, in case of α-emitting channels, different residues are expected to be populated via emission of different α clusters. The observed FRRDs were resolved into two Gaussian peaks, for αxn and αpxn channels, using the ORIGIN software. As a representative case, in Fig. 3(a) the measured RRD of evaporation residue ^{127}Cs shows two peaks at cumulative catcher thicknesses ≈1039 μg/cm^2 and ≈824 μg/cm^2 in the Al stopping medium. Here, the peak position at the smaller cumulative range ≈824 μg/cm^2 corresponds to the partial momentum transfer of the fragment ^{12}C from the projectile ^{16}O to the target, and may be due to the

TABLE II. Experimentally measured most probable ranges R_P^{expt} deduced from RRD curves, and theoretically calculated forward mean ranges R_P^{theor}, in Al in units of μg/cm^2 for the CF and ICF components using the SRIM code, produced in the interaction of ^{16}O with the ^{115}In target at 105 MeV. Experimentally measured forward recoil range integrated cross section $\sigma_{\text{expt}}^{RRD}$ deduced from RRD curves, and theoretically calculated cross section $\sigma_{\text{theor}}^{PACE4}$ at the studied energy.

Residues	$R^{CF}_{P(\text{expt})}$	$R^{CF}_{P(\text{theor})}$	$R^{ICF-^{12}C}_{P(\text{expt})}$	$R^{ICF-^{12}C}_{P(\text{theor})}$	$R^{ICF-^{8}Be}_{P(\text{expt})}$	$R^{ICF-^{8}Be}_{P(\text{theor})}$	$R^{ICF-^{4}He}_{P(\text{expt})}$	$R^{ICF-^{4}He}_{P(\text{theor})}$	$\sigma_{\text{expt}}^{RRD}$ (mb)	$\sigma_{\text{theor}}^{PACE4}$ (mb)
^{127}Ba	1003 ± 45	1053							39.9	30.9
^{126}Ba	1001 ± 32	1053							223.9	230.3
^{127}Cs	1039 ± 44	1053	824 ± 45	807					25.1	11.7
^{125}Cs	1018 ± 31	1053	788 ± 27	807					62.6	41.8
^{125}Xe	893 ± 33	1053	620 ± 22	807					19.4	10.5
^{123}Xe	999 ± 12	1053	647 ± 15	807					111.1	101.2
^{122}Xe	996 ± 28	1053	655 ± 12	807					49.6	25.1
^{121}I	1013 ± 34	1053	785 ± 21	807	534 ± 16	551			29.0	20.3
^{120}I^{g+m}	1022 ± 24	1053	793 ± 14	807	536 ± 10	551			98.7	37.1
^{119}I	963 ± 41	1053	780 ± 27	807	542 ± 26	551			6.2	1.2
^{118}Sb^{m}			791 ± 10	807	526 ± 14	551	288 ± 11	289	16.3	1.3
^{117}Sb			792 ± 23	807	514 ± 19	551	283 ± 13	289	18.1	1.5
^{116}Sb^{m}			789 ± 19	807	572 ± 15	551	324 ± 16	289	5.3	

ICF process. However, the peak position at larger cumulative catcher thickness ≈1039 μg/cm^2 corresponds to the expected recoil range of the compound system ^{131}La* via CF of ^{16}O with ^{115}In. This indicates that the reaction ^{115}In(^{16}O,α)^{127}Cs may be populated not only via CF but also via ICF. Therefore, both these reaction processes can be represented as

(i) CF of projectile ^{16}O, i.e.,

$$^{16}\text{O} + {}^{115}\text{In} \Rightarrow {}^{131}\text{La}^* \Rightarrow {}^{127}\text{Cs} + \alpha.$$

(ii) ICF of projectile ^{12}C, i.e.,

$$^{16}\text{O}[{}^{12}\text{C} + {}^{4}\text{He}] + {}^{115}\text{In} \Rightarrow {}^{127}\text{Cs}^* \Rightarrow {}^{127}\text{Cs}$$
(α as a spectator).

Similarly, in Figs. 3(b), 4(a), 4(b), and 4(c), the FRRDs of ^{125}Cs, ^{125}Xe, ^{123}Xe, and ^{122}Xe residues, respectively, show two peaks at different depths in the stopping medium, and hence the production of these residues can be described as for the ^{127}Cs residue. The experimentally estimated mean recoil ranges (R_P^{expt}) corresponding to these residues are exhibited in Table II along with their theoretically calculated projected ranges using SRIM code, and their normalized FWHM are also tabulated in Table III.

TABLE III. Comparison of normalized FWHM of the distributions.

Residues	CF	ICF_{α}	$ICF_{2\alpha}$	$ICF_{3\alpha}$
^{127}Ba	0.21			
^{126}Ba	0.22			
^{127}Cs	0.08	0.22		
^{125}Cs	0.11	0.23		
^{125}Xe	0.27	0.28		
^{123}Xe	0.16	0.35		
^{122}Xe	0.16	0.28		
^{121}I	0.07	0.19	0.40	
^{120}I^{g+m}	0.06	0.19	0.44	
^{119}I	0.06	0.18	0.44	
^{118}Sb^{m}		0.36	0.22	0.55
^{117}Sb		0.34	0.25	0.50
^{116}Sb^{m}		0.18	0.24	0.45

Further, in Fig. 5(a) there are three peaks observed in the FRRD, which indicates the three linear momentum components in this distribution. Hence, in the production of ^{121}I not only CF of ^{16}O but ICF of ^{12}C and ^{8}Be also takes place. The three peaks are obtained at depths 545, 772, and

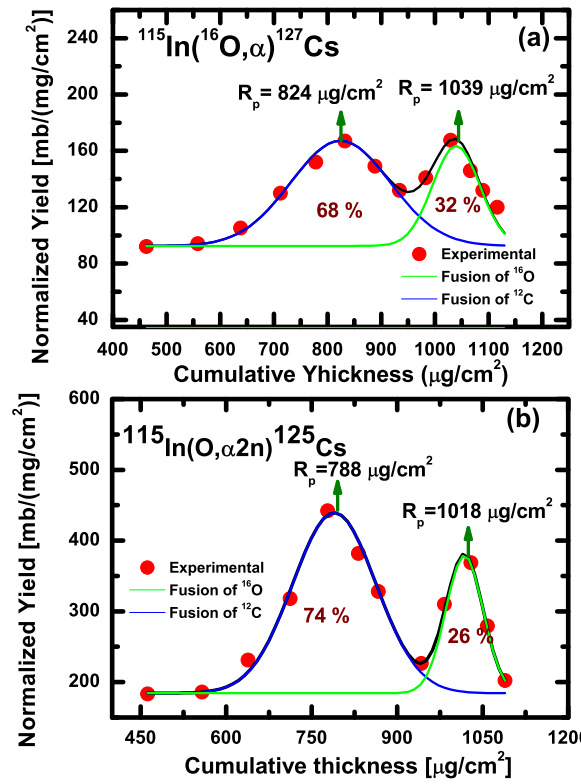

FIG. 3. (Color online) The experimentally measured recoil range distributions of (a) ^{127}Cs (α) and (b) ^{125}Cs ($\alpha 2n$) produced in the ^{16}O + ^{115}In system at 105 MeV energy.

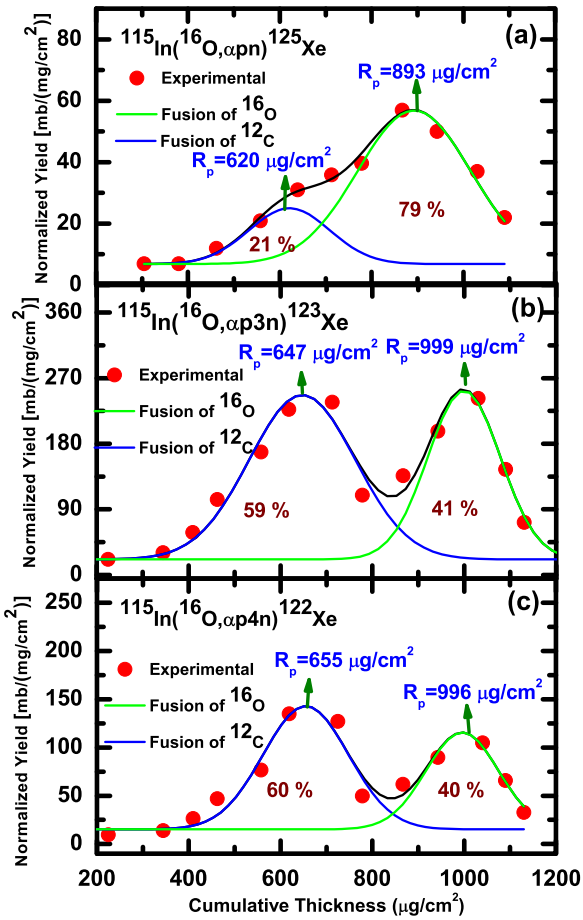

FIG. 4. (Color online) Experimentally measured recoil range distributions of (a) ^{125}Xe (αpn), (b) ^{123}Xe ($\alpha p3n$), and (c) ^{122}Xe ($\alpha p4n$) produced in the ^{16}O + ^{115}In system at 105 MeV energy.

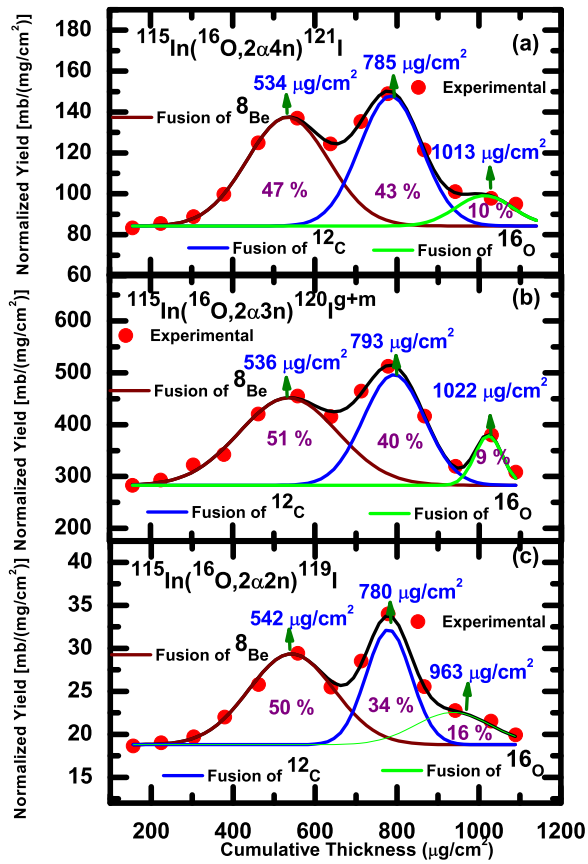

FIG. 5. (Color online) Experimentally measured recoil range distributions of (a) ^{121}I ($2\alpha 2n$), (b) ^{120}I^{g+m} ($2\alpha 3n$), and (c) ^{119}I ($2\alpha 4n$) produced in the ^{16}O + ^{115}In system at 105 MeV energy.

1015 μg/cm^2 for the fusion of ^{8}Be, ^{12}C, and ^{16}O, respectively, with the target ^{115}In. The associated reaction processes in the production of ^{121}I can also be represented as

(i) CF of projectile ^{16}O, i.e.,

$$^{16}\mathrm{O} + {}^{115}\mathrm{In} \Rightarrow {}^{131}\mathrm{La}^* \Rightarrow {}^{121}\mathrm{I} + 2\alpha + 2n.$$

(ii) ICF of ^{12}C, i.e.,

$$^{16}\mathrm{O}[{}^{12}\mathrm{C} + {}^{4}\mathrm{He}] + {}^{115}\mathrm{In} \Rightarrow {}^{127}\mathrm{Cs}^* \Rightarrow {}^{121}\mathrm{I} + \alpha + 2n$$

(α as a spectator).

(iii) ICF of ^{8}Be, i.e.,

$$^{16}\mathrm{O}[{}^{8}\mathrm{Be} + {}^{8}\mathrm{Be}] + {}^{115}\mathrm{In} \Rightarrow {}^{123}\mathrm{I}^* \Rightarrow {}^{121}\mathrm{I} + 2n$$

(2α or ^{8}Be as spectator).

In the same way, in Figs. 5(b) and 5(c), the FRRDs of ^{120}I^{g+m} and ^{119}I residues show three peaks at different depths in the stopping medium, and hence the production of these residues can be described as for the ^{121}I residue. The experimentally estimated mean recoil ranges (R_P^{expt}) corresponding to these residues are exhibited in Table II along with their theoretically calculated projected ranges using SRIM code, and their normalized FWHM are also listed in Table III.

In Figs. 6(a), 6(b), and 6(c), the recoil range distributions of the $3\alpha xn$ channels are shown. As a representative case, in Fig. 6(a), the FRRD of ^{118}Sb^m depicts three peaks at three different positions in the stopping medium. The comparison of these depths with SRIM calculations shows that all the three peaks are due to the ICF process, and the contribution due to CF is negligible. The possible reaction processes for the formation of ^{118}Sb^m can be represented as

(i) CF of projectile ^{16}O, i.e.,

$$^{16}\mathrm{O} + {}^{115}\mathrm{In} \Rightarrow {}^{131}\mathrm{La}^* \Rightarrow {}^{118}\mathrm{Sb}^m + 3\alpha + n.$$

(ii) ICF of ^{12}C, i.e.,

$$^{16}\mathrm{O}[{}^{12}\mathrm{C} + {}^{4}\mathrm{He}] + {}^{115}\mathrm{In} \Rightarrow {}^{127}\mathrm{Cs}^* \Rightarrow {}^{118}\mathrm{Sb}^m + 2\alpha + n$$

(α as a spectator).

(iii) ICF of ^{8}Be, i.e.,

$$^{16}\mathrm{O}[{}^{8}\mathrm{Be} + {}^{8}\mathrm{Be}] + {}^{115}\mathrm{In} \Rightarrow {}^{123}\mathrm{I}^* \Rightarrow {}^{118}\mathrm{Sb}^m + \alpha + n$$

(2α or ^{8}Be as spectator).

(iv) ICF of ^{4}He, i.e.,

$$^{16}\mathrm{O}[{}^{4}\mathrm{He} + {}^{12}\mathrm{C}] + {}^{115}\mathrm{In} \Rightarrow {}^{119}\mathrm{Sb}^* \Rightarrow {}^{118}\mathrm{Sb}^m + n$$

(3α or ^{12}C as spectator).

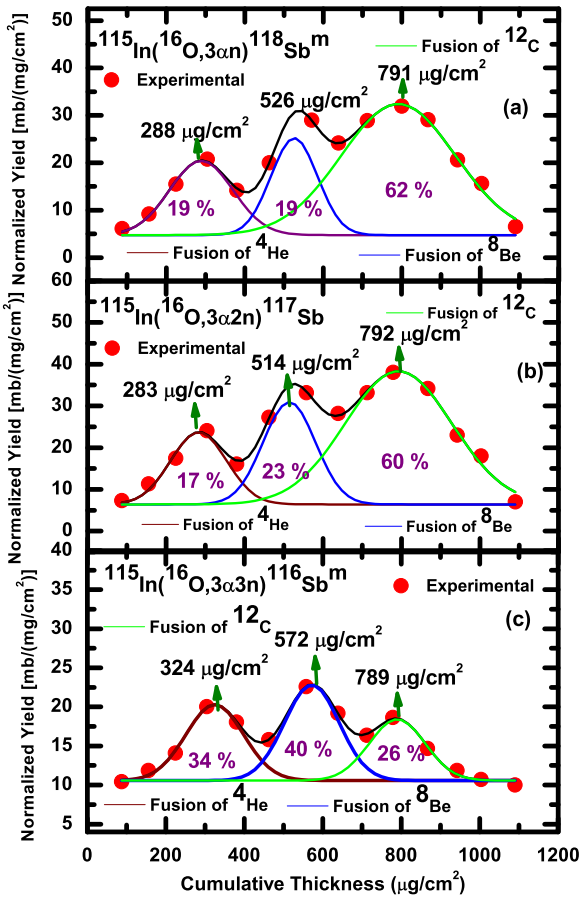

FIG. 6. (Color online) Experimentally measured recoil range distributions of (a) ^{118}Sb^{m} ($3\alpha n$), (b) ^{117}Sb ($3\alpha 2n$), and (c) ^{116}Sb^{m} ($3\alpha 3n$) produced in the ^{16}O + ^{115}In system at 105 MeV energy.

Similarly, the formation processes of ^{117}Sb and ^{116}Sb^{m} residues can also be described. The estimated projected ranges of these residues are shown along with those of theoretically calculated ranges using SRIM code in Table II, and their normalized FWHMs are also shown in Table III. In order to compare the range integrated yields of CF and ICF reactions, the statistical model calculations were carried out using the code PACE4 [40]. This model follows the correct procedure for angular momentum coupling at each stage of deexcitation. The angular momentum conservation is explicitly taken into account at each step. For any specific bombarding energy, the partial cross section for CN formation at angular momentum ℓ, σ_ℓ, is

$$\sigma_\ell = \frac{\lambda^2}{4\pi}(2\ell+1)T_\ell. \tag{3}$$

where λ is the reduced wave length, and T_ℓ, the transmission coefficient, is given by the expression

$$T_\ell = \left[1+\exp\left(\frac{\ell-\ell_{\max}}{\Delta}\right)\right]^{-1}, \tag{4}$$

where Δ is a diffuseness parameter and $\ell_{\max}$, the maximum amount of ℓ detained by total fusion cross section, is determined by

$$\sigma_F = \Sigma\sigma_\ell \tag{5}$$

The transmission coefficients for the emission of light particles (n, p, and α) during the deexcitation were determined using optical model calculations [41,42]. In this calculation the input fusion cross section was calculated using the Bass formula [43]. In the description of γ-ray competition, emission of E_1, E_2, M_1, and M_2 γ rays are included, and the γ-ray strength functions for different transitions are taken from the tables of Endt [44].

The relative contributions of complete and incomplete fusion in the production of a particular reaction product may be computed by fitting the experimentally measured RRDs with a Gaussian distribution using the ORIGIN software. The Gaussian yield curves of evaporation residues obtained from RRD are given by

$$Y = Y_o + \frac{A}{\omega_A^2\sqrt{2\pi}}\exp^{-(R-R_P)^2/2\pi\omega_A^2}, \tag{6}$$

where A is the area under peak, ω_A is the width parameter (FWHM) of the distribution, and R_p is the most probable mean range. Further, the normalized yield Y may be estimated by the χ-square fit (χ^2) of the experimentally determined range distributions and may be represented as follows:

$$\chi^2 = \frac{1}{(m-p-1)}[Y(A)-Y_o(A)]^2. \tag{7}$$

The value of χ^2 was minimized in this analysis using a nonlinear least-squares fit routine, keeping the width parameter (ω_A) and the most probable mean range (R_p) in the FRRD as a free parameter. Moreover, as indicated in Figs. 3–6, the residues involving α-emitting channels show more than one RRD component. In such cases, the experimentally measured normalized yields were fitted using the multipeak option in the ORIGIN software as mentioned above. The relative contributions of different fusion components to the formation of a residue were obtained by dividing the area under the peak of the corresponding fusion component by the total area of all the peaks in the distribution. As a representative case, in Fig. 5(c) the relative contributions due to fusion of fragments ^{8}Be, ^{12}C, and ^{16}O are found to be 50%, 34%, and 16%, respectively. The relative contributions of the CF and various ICF channels for each residue were estimated, and are shown in the respective figures. The details of various factors that may introduce errors and uncertainties in the present cross-sectional measurements are given in our previous observation [30]. The overall errors in the measured cross sections are expected to be less than 15%.

IV. DEPENDENCE OF ICF ON PROJECTILE ENERGY AND MASS ASYMMETRY OF INTERACTING PARTNERS

In the present work, it has been observed that the contribution of CF satisfactorily matches that predicted by the PACE4 code [40] with physically reasonable parameters, as in our recent observation [30], which were optimized to reproduce the evaporation residues populated in the case of complete fusion reactions such as pxn channels. However, the cross sections of ICF channels could not be reproduced by the PACE4 code (as shown in Table II) by using the same set of parameters, since PACE4 does not take ICF in to account. Moreover, to study the dependence of ICF on various entrance channel parameters,

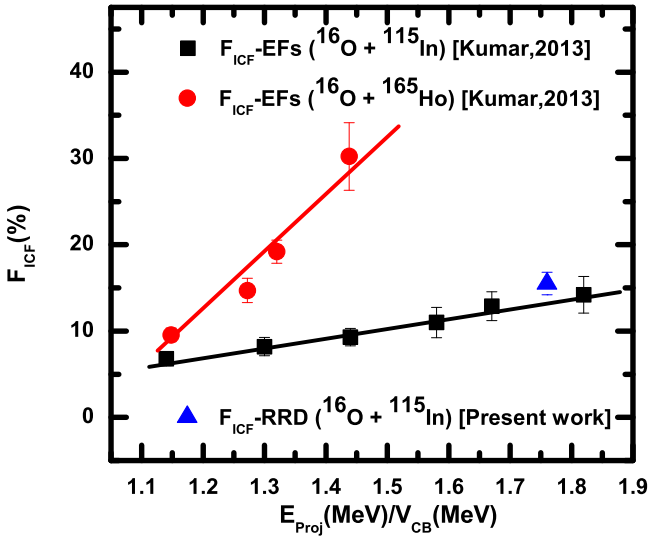

FIG. 7. (Color online) The incomplete fusion fractions (F_{ICF}) deduced from Kumar's analysis of EFs [30,35] are shown. The deduced F_{ICF} of the present FRRD analysis is also shown.

the percentage ICF fraction (F_{ICF}) is evaluated using the relation

$$F_{ICF} = \frac{\Sigma\sigma_{ICF}}{\Sigma\sigma_{CF} + \Sigma\sigma_{ICF}} \times 100 \qquad (8)$$

where $\Sigma\sigma_{CF}$ and $\Sigma\sigma_{ICF}$ are the sums of complete and incomplete fusion cross sections, respectively, at the studied energies. The value of F_{ICF} obtained from the excitation function measurements of the same system $^{16}O + ^{115}In$ [30], as a function of normalized projectile energy (E_{proj}/V_{CB}), is plotted in Fig. 7. As can be seen from this figure, the F_{ICF} increases with the projectile energy. Moreover, it can also be seen that the F_{ICF} deduced from present FRRD data lies on the same line, which supports the present measurement and analysis. Further, the deduced F_{ICF} from our earliar measurement [35] is also plotted in Fig. 7, with respect to the normalized projectile energy. From this figure, it can be seen that the percentage ICF contribution for the system $^{16}O + ^{165}Ho$ [35] increases more rapidly than that of the system $^{16}O + ^{115}In$ [30], which can be understood in terms of mass-asymmetry systematics of interacting partners, introduced by Morgenstern *et al.* [45]. According to the mass-asymmetry systematics, the ICF probability should be more for more a mass-asymmetric system thanfor a mass symmetric system. The mass asymmetry of any system can be denoted as $M_a = A_T/(A_T + A_P)$, where A_T and A_P are the masses of the target and of the projectile, respectively. Hence, the calculated mass asymmetries of the systems $^{16}O + ^{115}In$ and $^{16}O + ^{165}Ho$ are 0.877 and 0.911, respectively. Therefore, Fig. 7 reflects that these two systems follow the mass-asymmetry systematics even at low incident energies, while Morgenstern *et al.* [45] observed this systematics at relatively higher energies $\approx$ 10 to 25 MeV/nucleon. Moreover, this rapid increase in Fig. 7 can also be explained by the systematics introduced by Gomes *et al.* [46], which shows dependence of ICF on Coloumb repulsion ($Z_P \times Z_T$) of the interacting partners. Hence, the larger Coloumb repulsion in the $^{16}O + ^{165}Ho$ system than in the $^{16}O + ^{115}In$ system leads to a higher probability for ICF. Also, it was observed by Inamura *et al.* [23] that ICF processes are mainly due to the peripheral interactions. This situation may also be one of the reasons for the rapid increase, due to the larger angular momenta associated with the system $^{16}O + ^{165}Ho$ than that associated with the system $^{16}O + ^{115}In$.

V. PROJECTILE STRUCTURE DEPENDENCE OF ICF REACTION DYNAMICS

In our recent observations [30,35], we observed a strong dependence of projectile breakup on the projectile structure in the nuclear field of the same target. These studies were carried out using ^{115}In and ^{165}Ho targets, which are relatively medium and higher mass targets. Hence, we have made an attempt to study the projectile structure dependence of ICF reactions in the nuclear field of a low mass target. The breakup of different projectiles in the nuclear field of the same target can be understood in terms of the α-Q value of projectile. In Fig. 8, we have plotted the F_{ICF} for the three different systems, i.e., $^{16}O + ^{165}Ho$ [35], $^{12}C + ^{165}Ho$ [47], and $^{20}Ne + ^{165}Ho$ [48] with respect to the α-Q values of the projectiles at a constant relative velocity (i.e., $v_{rel} = 0.055c$). The α-Q values of the three projectiles, i.e., ^{12}C, ^{16}O, and ^{20}Ne are -7.37, -7.16, and -4.73 MeV, respectively, make ^{20}Ne more unstable for breakup in the nuclear field of the same target. From Fig. 8, it can be seen that the ^{12}C induced reaction possesses the lowest F_{ICF}, while the ^{20}Ne induced reaction possesses the highest F_{ICF} among the three reactions. However, according to the mass-asymmetry systematics the ICF contribution of the $^{12}C + ^{165}Ho$ system should be maximum among the three systems, and that of $^{20}Ne + ^{165}Ho$ system should be minimum. Hence, we found that the projectile structure effect predominately depends on the α-Q value of the projectile when the target is the same. In order to see the dependence of ICF

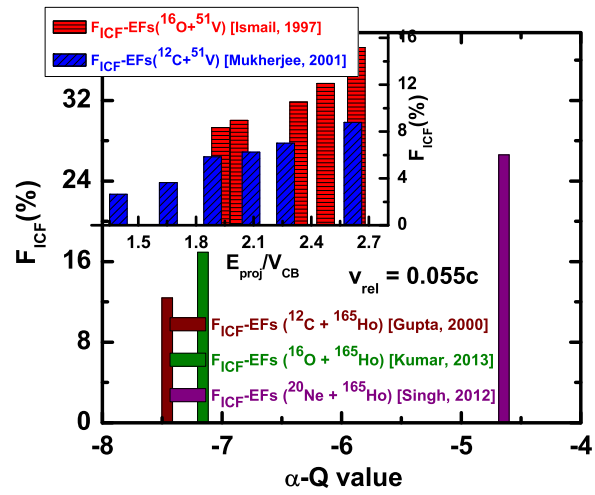

FIG. 8. (Color online) Deduced percentage ICF fraction F_{ICF} as a function of α-Q value for systems $^{12}C + ^{165}Ho$ (Gupta [47]), $^{16}O + ^{165}Ho$ (Kumar [35]), and $^{20}Ne + ^{165}Ho$ (Singh [48]). In the inset, deduced F_{ICF} of two other systems, $^{16}O + ^{51}V$ (Mukherjee [49]) and $^{12}C + ^{51}V$ (Ismail [50]), are shown.

reactions on the projectile structure effect and the α-Q value of the projectile in the nuclear field of a low mass target, we have studied two other systems, $^{12}C + ^{51}V$ [49] and $^{16}O + ^{51}V$ [50], which correspond to a relatively low mass target ^{51}V. In the inset of Fig. 8, the estimated F_{ICF} of these systems has been plotted against the normalized projectile energy. From this figure, we can see that the $^{16}O + ^{51}V$ system possesses a greater ICF contribution than that of $^{12}C + ^{51}V$ system. Therefore, it can be concluded that the projectile structure effect and the α-Q value of projectile both are responsible for the ICF reaction dynamics, even in the low-mass target region.

VI. CONCLUSIONS

The recoil range distributions of evaporation residues ^{127}Ba($p3n$), ^{126}Ba($p4n$), ^{127}Cs(α), ^{125}Cs($\alpha 2n$), ^{125}Xe(αpn), ^{123}Xe($\alpha p3n$), ^{122}Xe($\alpha p4n$), ^{121}I($2\alpha 2n$), ^{120}I^{g+m}($2\alpha 3n$), ^{119}I($2\alpha 4n$), ^{118}Sb^{m}($3\alpha n$), ^{117}Sb($3\alpha 2n$), and ^{116}Sb^{m}($3\alpha 3n$) were measured in the $^{16}O + ^{115}$In interaction, at $\approx$ 105 MeV beam energy. The measured forward recoil ranges of reaction products strongly revealed a significant contribution from the partial and entire linear momentum transfers of the projectiles associated with the complete and incomplete fusion, respectively. Different fusion components are attributed to ^{12}C and/or ^{8}Be transfer from the ^{16}O projectile to the target nucleus. The relative contributions of complete and/or incomplete fusion components were also evaluated. The present analysis shows that both complete as well as incomplete fusion play an important role in the production of different reaction products involving direct α-cluster emission at low energies. The above measurements are also consistent with the theoretical predictions based on the statistical model code PACE4. Moreover, dependence of ICF reaction dynamics on different entrance channel parameters, i.e., projectile energy, mass asymmetry of the interacting partners, α-Q value of the projectile, and the projectile structure effect, was observed.

ACKNOWLEDGMENTS

The authors thank the IUAC, New Delhi, India, for immense support during the experiment and analysis. We sincerely thank the Department of Physics, AMU, Aligarh, India for providing all necessary facilities. Authors K.K. and S.A. extend their gratitude towards U.G.C. for financial support.

[1] P. Vergani *et al.*, Phys. Rev. C **48**, 1815 (1993).
[2] D. J. Parker, J. J. Hogan, and J. Asher, Phys. Rev. C **35**, 161 (1987).
[3] F. K. Amanuel, B. Zelalem, A. K. Chaubey, A. Agarwal, I. A. Rizvi, A. Maheshwari, and T. Ahmed, Phys. Rev. C **84**, 024614 (2011).
[4] D. P. Singh, U. Gupta, P. P. Singh, A. Yadav, M. K. Sharma, B. P. Singh, K. S. Golda, R. Kumar, A. K. Sinha, and R. Prasad, Phys. Rev. C **80**, 014601 (2009).
[5] F. Amorini *et al.*, Phys. Rev. C **58**, 987 (1998).
[6] A. Yadav, V. R. Sharma, P. P. Singh, D. P. Singh, M. K. Sharma, U. Gupta, R. Kumar, B. P. Singh, R. Prasad, and R. K. Bhowmik, Phys. Rev. C **85**, 034614 (2012).
[7] V. V. Sargsyan, A. S. Zubov, G. G. Adamian, N. V. Antonenko, and S. Heinz, Phys. Rev. C **88**, 054609 (2013).
[8] W. Loveland, Phys. Rev. C **76**, 014612 (2007).
[9] V. I. Zagrebaev *et al.*, Nucl. Phys. A **734**, 164 (2004).
[10] R. Smolańczuk, Phys. Rev. C **59**, 2634 (1999).
[11] I. M. Itkis *et al.*, Phys. Rev. C **83**, 064613 (2011).
[12] S. Heinz *et al.*, Eur. Phys. J. A **43**, 181 (2011).
[13] K. Nishio *et al.*, Phys. Rev. C **77**, 064607 (2008).
[14] F. K. Amanuel *et al.*, Eur. Phys. J. A **47**, 156 (2010).
[15] A. Agarwal *et al.*, Eur. Phys. J. Web Conf. **38**, 17001 (2012).
[16] M. Dasgupta *et al.*, Phys. Rev. C **70**, 024606 (2004).
[17] L. F. Canto, R. Donangelo, L. M. de Matos, M. S. Hussein, and P. Lotti, Phys. Rev. C **58**, 1107 (1998).
[18] B. B. Kumar *et al.*, Phys. Rev. C **59**, 2923 (1999).
[19] P. P. Singh *et al.*, Phys. Rev. C **80**, 064603 (2009).
[20] A. Agarwal *et al.*, Int. J. Mod. Phys. E **17**, 393 (2008).
[21] H. C. Britt and A. R. Quinton, Phys. Rev. **124**, 877 (1961).
[22] J. Galin *et al.*, Phys. Rev. C **9**, 1126 (1974).
[23] T. Inamura *et al.*, Phys. Lett. B **68**, 51 (1977).
[24] R. Weiner *et al.*, Nucl. Phys. A **286**, 282 (1977).
[25] J. Wilczynski *et al.*, Nucl. Phys. A **373**, 109 (1982).
[26] T. Udagawa and T. Tamura, Phys. Rev. Lett. **45**, 1311 (1980).
[27] M. Blann, Phys. Rev. C **31**, 295(R) (1985).
[28] J. P. Bondrof, Nucl. Phys. A **333**, 285 (1980).
[29] D. J. Parker, J. J. Hogan, and J. Asher, Phys. Rev. C **39**, 2256 (1989).
[30] K. Kumar, T. Ahmad, S. Ali, I. A. Rizvi, A. Agarwal, R. Kumar, and A. K. Chaubey, Phys. Rev. C **88**, 064613 (2013).
[31] A. Yadav *et al.*, Phys. Rev. C **85**, 064617 (2012).
[32] H. Tricoire *et al.*, Z. Phys. A **306**, 127 (1982).
[33] T. Ahmad *et al.*, Int. J. Mod. Phys. E **20**, 645 (2011).
[34] D. J. Hinde *et al.*, Phys. Lett. B **89**, 272701 (2002).
[35] K. Kumar *et al.*, Phys. Rev. C **87**, 044608 (2013).
[36] A. Yadav *et al.*, Phys. Rev. C **86**, 014603 (2012).
[37] B. P. Ajith Kumar *et al.*, *CANDLE, Collection and Analysis of Nuclear Data using Linux Network* (DAE SNP, Kolkata, 2001).
[38] E. Browne and R. B. Firestone, *Table of Radioactive Isotopes* (Wiley, New York, 1986).
[39] The Stopping and Range of Ions in Matter (SRIM) code: http://www.srim.org/SRIM/SRIMLEGL.htm
[40] A. Gavron, Phys. Rev. C **21**, 230 (1980).
[41] F. D. Becchetti and G. W. Greenlees, Phys. Rev. **182**, 1190 (1969).
[42] G. R. Satchler, Nucl. Phys. **70**, 177 (1965).
[43] R. Bass, Nucl. Phys. A **231**, 45 (1974).
[44] P. M. Endt, At. Data Nucl. Data Tables **26**, 47 (1981).
[45] H. Morgenstern, W. Bohne, W. Galster, K. Grabisch, and A. Kyanowski, Phys. Rev. Lett. **52**, 1104 (1984).
[46] P. R. S. Gomes *et al.*, Phys. Rev. C **73**, 064606 (2006); Phys. Lett. B **601**, 20 (2004).
[47] S. Gupta, B. P. Singh, M. M. Musthafa, H. D. Bhardwaj, and R. Prasad, Phys. Rev. C **61**, 064613 (2000).
[48] D. Singh *et al.*, Nucl. Phys. A **879**, 107 (2012).
[49] S. Mukherjee *et al.*, Eur. Phys. J. A **12**, 199 (2001).
[50] M. Ismail *et al.*, Pramana J. Phys. **49**, 623 (1997).